Electronic, structural, and optical properties of crystalline yttria

Yong-Nian Xu
Department of Physics, University of Missouri-Kansas City, Kansas City, Missouri 64110

Zhong-quan Gu
National Laboratory for Surface Science and Institute of Semiconductors, Chinese Academy of Sciences, Beijing, People's Republic of China

W. Y. Ching*
Max-Planck-Institut für Metallforschung, Seestrasse 92, D-70174 Stuttgart, Germany and Department of Physics, University of Missouri-Kansas City, Kansas City, Missouri 64110
(Received 11 June 1997)

The electronic structure of crystalline Y_2O_3 is investigated by first-principles calculations within the local-density approximation (LDA) of the density-functional theory. Results are presented for the band structure, the total density of states (DOS), the atom- and orbital-resolved partial DOS, effective charges, bond order, and charge-density distributions. Partial covalent character in the Y-O bonding is shown, and the nonequivalency of the two Y sites is demonstrated. The calculated electronic structure is compared with a variety of available experimental data. The total energy of the crystal is calculated as a function of crystal volume. A bulk modulus B of 183 Gpa and a pressure coefficient B' of 4.01 are obtained, which are in good agreement with compression data. An LDA band gap of 4.54 eV at Γ is obtained which increases with pressure at a rate of $dE_g/dP = 0.012$ eV/Gpa at the equilibrium volume. Also investigated are the optical properties of Y_2O_3 up to a photon energy of 20 eV. The calculated complex dielectric function and electron-energy-loss function are in good agreement with experimental data. A static dielectric constant of $\varepsilon(0) = 3.20$ is obtained. It is also found that the bottom of the conduction band consists of a single band, and direct optical transition at Γ between the top of the valence band and the bottom of the conduction band may be symmetry forbidden. [S0163-1829(97)06547-8]

I. INTRODUCTION

Yttria (Y_2O_3), together with alumina (Al_2O_3), are the two most important sesquioxides within the general class of refractory ceramics. Y_2O_3 has many applications such as sintering aids in the processing of ceramic materials, substrates for semi-conducting films, optical windows, and components for rare-earth doped lasers, etc. It is well known that a small addition of Y_2O_3 influences both the properties and the microstructures of Al_2O_3, the so-called yttrium effect;[1,2] and Y has a beneficial effect of increasing the adhesion oxide scales in all Al-containing metals.[3,4] Many of the unique properties of yttria and yttria-related materials depend critically on the defect structures and their concentrations,[5] and on the formation of intermediate phases.[6] There are three intermediate compounds of very different crystal structures between Y_2O_3 and Al_2O_3, $YAlO_3$ (YAP), $Y_3Al_5O_{12}$ (YAG), and $Y_2Al_2O_9$ (YAM). Their electronic structures are yet unknown. It is therefore important to study first the electronic structure and bonding in crystalline Y_2O_3 at the microscopic level before any of the more challenging problems in the yttria-related materials can be tackled.

In comparison to α-Al_2O_3, the study of the electronic structure in the Y_2O_3 system has received much less attention. Only limited experimental measurements were carried out,[7–10] and theoretical support in the interpretation of these data were totally lacking. Part of the reason is due to the rather complex crystal structure of Y_2O_3, and the complication with the presence of the defects in the samples. In recent years, fundamental research on ytteria has increased both in theory[11,12] and in experiment.[12–16] However, a complete understanding of the electronic structure and bonding in yttria has not been fully attained. For example, there is ample evidence that a formal charge description of Y^{3+} and O^{2-} is not appropriate for the system, yet such a concept of long historical standing has been conveniently used in models to account for many experimental data on diffusion, transport, and thermodynamic phase equilibria.

In 1990, we published a self-consistent band-structure calculation of Y_2O_3,[11] using the orthogonalized linear combination of atomic orbitals (OLCAO) method in the local density approximation (LDA) of the density-functional theory. The unique type of bonding in Y_2O_3 was emphasized, and a partial charge description of $Y_2{}^{+2.16}O_3{}^{-1.44}$ was concluded. Also studied were the optical properties of Y_2O_3. In the present paper, we present improved results on that study, with a more thorough description of the methodology used and a detailed discussion of results. Also included are results on the total-energy calculation for Y_2O_3. We also compare our results with some of the more recent experiments, and with the other recent first-principles calculation.[12] In Sec. II, the crystal structure of Y_2O_3 is discussed first. This is followed by a description of the method used in the calculation. In Sec. IV, the main results on band structure, density of states (DOS), atom- and orbital-resolved partial DOS (PDOS), effective charges, bond order, and charge-density distributions,

total energy, and optical properties are presented and discussed. In the last section, brief conclusions are made, and possible future work along the direction of this study is proposed.

II. CRYSTAL STRUCTURE OF Y_2O_3

The crystal structure for yttria is sketched in Fig. 1. Although there are several more recent determinations of the crystal structure of Y_2O_3,[16–18] we find the differences with the older data are quite small. For consistency, we used the crystal data with a lattice constant of 10.604 Å as provided by Wyckoff.[19] Y_2O_3 has a cubic structure of space group $Ia3\text{-}(T_h^7)$ (No. 206). The unit cell contains two inequivalent cation sites, Y1 at the $8a$ site and Y2 at the $24d$ site, and one type of O at the $48e$ site. The cubic cell contains a total of 80 atoms. The fluoritelike structure, named after the mineral bixbyite, can best be viewed as consisting of 64 slightly distorted minicubes with Y atoms sitting at the centers of 32 of the minicubes. The O atoms are at six of the eight corners of the cube such that an approximate octahedral coordination for the cation is maintained. The missing O are either at the face diagonal (75%) or at the end of the body diagonal (25%) of the minicube. For minicubes having Y1 at the center, three O are at one face of the cube, and the other three O are at the opposite face. There are six equal Y1-O bonds of 2.261 Å. For minicubes containing Y2, four O are at one face and the other two at the opposite face. There are three different pairs of Y2-O bonds of 2.249, 2.278, and 2.336 Å in length. On average, the Y1-O bonds are slightly shorter than the Y2-O bonds. Each O atom is linked to one Y1 and three Y2 atoms in the form of a distorted tetrahedron. The shortest O-O separations are 2.865 and 2.927 Å.

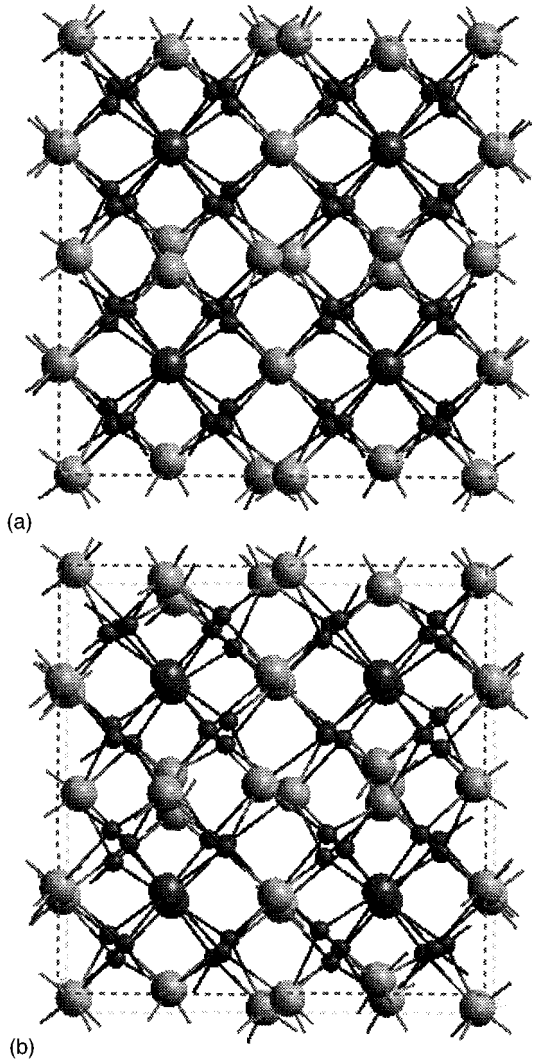

FIG. 1. Crystal structure of Y_2O_3. (a) Along the [001] direction. (b) In a direction slightly deviated from [001]. The large light (dark) ball is for Y1 (Y2), and the smaller ball is for O.

III. METHOD OF CALCULATION

We used the OLCAO method to calculate the electronic structure of Y_2O_3. This method has been described in some detail before,[20] and has been successfully applied in studies of the electronic structure of solids including many other ceramic crystals such as $\alpha\text{-}Al_2O_3$,[21,22] MgO,[21] $MgAl_2O_4$,[21] ZrO_2,[23] α- and $\beta\text{-}Si_3N_4$[24] and Si_2N_2O.[24] More recently, it has been used to investigate the O vacancy (Ref. 25) and Y substitutional impurity[26] in $\alpha\text{-}Al_2O_3$, using a supercell approach. Here we present only the essential steps in the calculation that are pertinent to the Y_2O_3 study. We used a full basis set which includes the minimal basis set (core orbitals plus Y $5s$, Y $5p$, Y $4d$, O $2s$ and O $2p$) plus additional excited state orbitals (O $3s$, O $3p$, Y $6s$, Y $6p$, and Y $5d$). In the previous study,[11] a near-minimal basis set including Y $5d$ orbitals was used. We applied a rather arbitrary criterion of considering any state whose energy is lower than the O $2s$ level as a core state. Hence Y $4p$ was treated as a core state and frozen in the present calculation. All atomic orbitals were expanded in terms of Gaussian types of orbitals (21 terms for Y, 17 terms for O) with orbital exponents ranging from 0.12 to 0.1×10^7. The crystal potential and the charge density were represented by the sums of atom-centered functions, which were also expressed as combinations of s-type Gaussians. The accuracy of the potential representation was improved by treating the functions centered at the Y1 and Y2 sites as independent, and by a more judicious choice of the fitting functions. The crystal potential was constructed according to the usual LDA formalism. The Wigner interpolation formula was used for the exchange-correlation potential. No attempts were made to use other forms of exchange-correlation potential or to go beyond the LDA. Ten special **k** points were used in self-consistent iterations with the convergence reached in less then 20 iterations. The energy eigenvalues and the Bloch wave functions were obtained at 55 regularly spaced **k** points in the irreducible portion of the Brillouin zone (BZ) by straightforward matrix diagonalization. Because of the large unit cell, this number of **k**-point samplings is a adequate. *Ab initio* wave functions were used to calculate the effective charges, bond order, and optical properties, and for the partial decomposition of the DOS. Test calculations were carried out with different levels of **k**-point sampling for both Y_2O_3 and $\alpha\text{-}Al_2O_3$. For the DOS calculation, the present level of sampling is more than sufficient. For optical calculations, we find the present level of **k**-point sampling is also adequate in the sense that no dis-

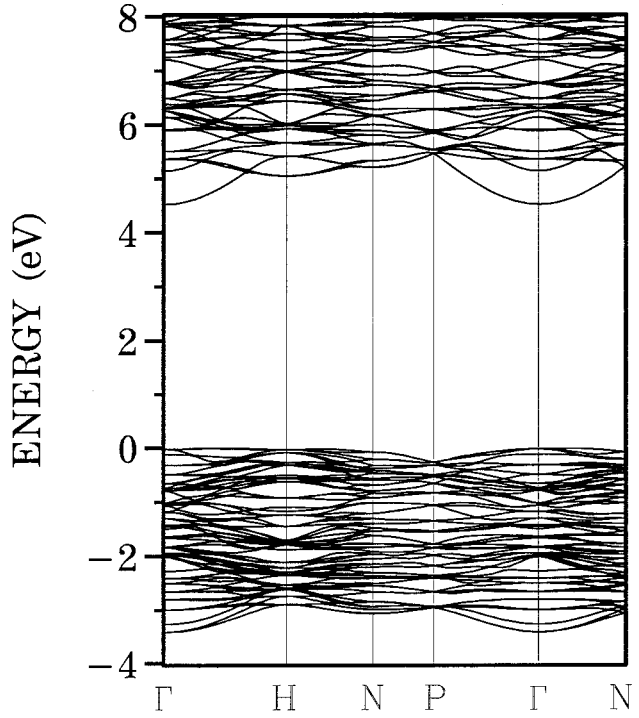

FIG. 2. Calculated band structures of Y_2O_3.

cernible differences were noted when the number of **k** points were increased.

In the OLCAO method, it is natural to define the effective charge $Q_\delta^* = \Sigma_\gamma \rho_{\gamma,\delta}$ on atom δ by the overlap population $\rho_{\gamma,\delta}$ between atoms γ and δ, using the Mulliken scheme[27]

$$\rho_{\gamma,\delta} = \sum_{n=\text{occ.}} \sum_i \sum_j \sum_k W(\mathbf{k}) (A^n_{i,\gamma})^* A^n_{j,\delta} S_{i\gamma,j\delta}(\mathbf{k}), \quad (1)$$

where $W(\mathbf{k})$ is the **k**-point weighting factor. The summations over **k** is for the entire BZ and over n is for all occupied states. $A_{i,\gamma}$ are the wave function coefficients. $S_{i,\gamma,j\delta}(\mathbf{k})$ are the overlap integrals between the Bloch functions at **k**, i and j are the orbital specifications for atoms γ and δ, respectively. Since the Mulliken scheme works best when the basis functions are relatively localized, the calculations for Q_δ^* and $\rho_{\gamma,\delta}$ are based on a separate minimal basis calculation for Y_2O_3.

The total energy E of the crystal is part of the self-consistent LDA calculation. We simply repeated the calculation with different lattice constant or volume (V) to obtain the $E(V)$ relation for Y_2O_3. This is a reasonable approximation for the case of hydrostatic pressure applied to a cubic crystal like Y_2O_3. The accumulated E vs V data were fitted to three types of equations of state (EOS's) for the bulk modulus B and the pressure coefficient B': (1) a fourth-order polynomial expansion in V; (2) the Murnagan EOS (Ref. 28); and (3) the Birch-Murnagan EOS.[29] Our past experience with many crystalline systems indicates that the total-energy calculation using a minimal basis set is not sufficient to predict the equilibrium volume and bulk modulus of the crystal accurately because of the limited variational freedom. Accuracy generally improves when more orbitals are added. At the full basis level (as explained above), the total energy values are well converged. Additional augmentation of the basis set makes only a marginal difference, but at the risk of running into numerical problems associated with the linear dependency of the basis set.

The frequency-dependent interband optical conductivity $\sigma(\omega)$ is calculated according to

$$\sigma(\hbar\omega) = \frac{e^2}{(2\pi)^2 \mu \hbar \omega} \int d\mathbf{k} \sum_{n,m} |\langle \psi_m(\mathbf{k},\mathbf{r}) | \mathbf{p} | \psi_n(\mathbf{k},\mathbf{r}) \rangle|^2 \times f_n(\mathbf{k})[(1 - f_m(\mathbf{k})] \delta[E_m(\mathbf{k}) - E_n(\mathbf{k}) - \hbar\omega], \quad (2)$$

where $\Psi_m(\mathbf{k},\mathbf{r})$ is the Block function for the mth band at **k**. $\hbar\omega$ is the photon energy, and f_n is the Fermi function for the state n. The optical matrix elements were evaluated at each **k** point using the *ab initio* wave functions. Integration over the BZ was performed using the linear analytic tetrahedron method. In the present calculation, because the semicore Y: $4p$ state was frozen and not considered in the optical transition, we restricted our optical calculations to photon energies below 20 eV. From $\sigma(\omega)$, the imaginary part of the dielectric function $\epsilon_2(\omega)$ is obtained from $\epsilon_2(\omega) = (4\pi/\omega)\sigma(\omega)$. The real part of the dielectric function $\epsilon_1(\omega)$ is extracted from $\epsilon_2(\omega)$ using the Kramers-Kronig relation. The electron-energy-loss function is derived from the complex dielectric function. We find the **k**-space convergence is more stringent in the optical spectrum calculation than for the DOS calculation. The present calculation is based on 55 **k** points in 1/48th of the BZ. The computational burden for optical calculations in a complex crystal such as Y_2O_3 is rather heavy because a large number of pairs of transitions between the occupied valence-band (VB) states and the unoccupied conduction-band (CB) states must be considered.

IV. RESULTS

A. Electronic structure and bonding

Calculated band structures along the high-symmetry axes of the BZ for Y_2O_3 are shown in Fig. 2. This band structure, characterized by a flat top in the VB, and a single band at the bottom of the CB, is similar to the previous one,[11] with two exceptions. The calculated direct LDA gap of 4.54 eV at Γ is larger than the previous calculation because of a more accurate treatment in the potential representation. This gap is the same as that of Ref. 12 calculated using the linear muffin-tin orbital (LMTO) method. Actually, we find the top of the VB to be along the direction from Γ to H. However, the difference in their energies is negligibly small. There are more CB's now because of a more extended basis set used. The

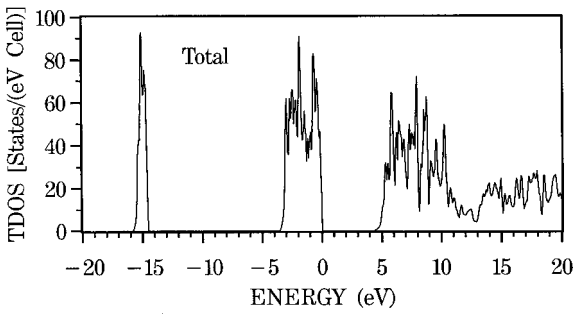

FIG. 3. Calculated total DOS of Y_2O_3.

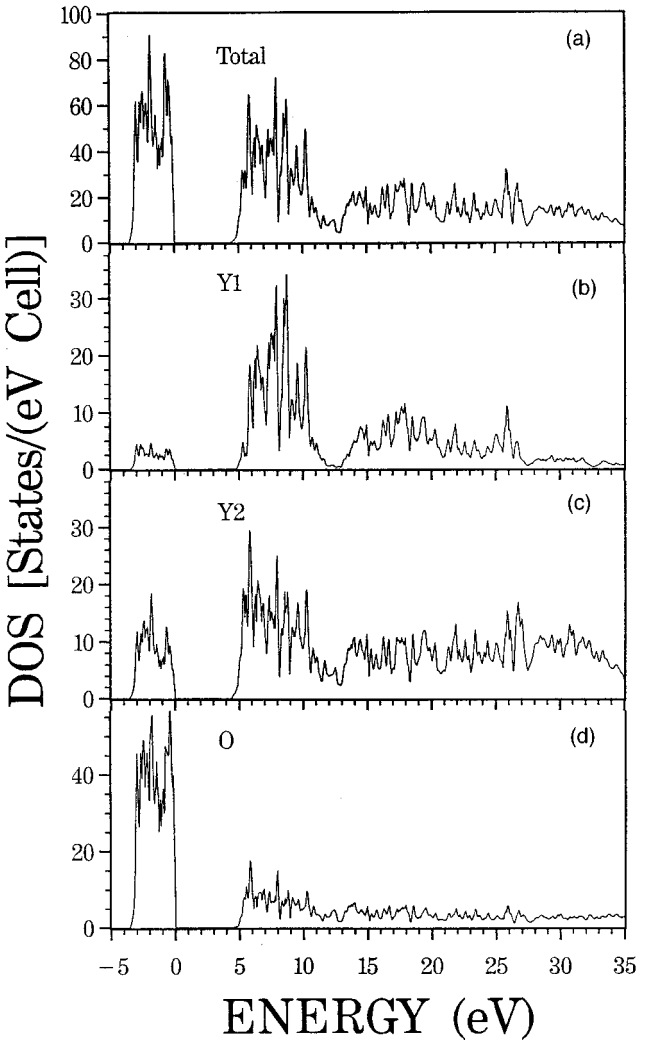

FIG. 4. Atom-resolved PDOS of Y_2O_3. (a) Total. (b) Y1. (c) Y2. (d) O.

calculated total DOS is presented in Fig. 3. The major features can be summarized as follows. (1) The upper VB has a width of 3.5 eV and has multiple structures. Roughly speaking, three peak structures at -0.5, -2.0 and -2.5 eV can be identified. (2) The lower O $2s$ band is centered at -15 eV, and has a width of about 1.3 eV. The CB DOS has most of the states in the 5–11-eV range. Above 11 eV, there are no significant structures. It should be noted that although the calculated minimal gap is 4.5 eV, the CB edge has a footlike structure due to a single CB dipping down at Γ, so the steeper part of the CB starts at 5.0 eV. This feature is very similar to α-Al_2O_3.[22]

To compare with recent soft-x-ray emission spectroscopy (XES) (Ref. 12) and x-ray-absorption spectroscopy (XAS) measurements,[13,14] we resolved the total DOS of Y_2O_3 into its atomic and orbital components, which are presented in Figs. 4–7 for energy ranges from -5 to 35 eV. The main results can be summarized as follows: (1) The upper VB is mainly derived from O $2p$ orbitals, with some mixing from Y $4d$ at the low-energy side and Y $5p$ at the high-energy side. (2) The s orbitals of Y and O make very small contributions to the upper VB. In the lower CB region, Y1 s has a higher contribution than Y2. (3) From the standing point of the PDOS the difference between Y1 (25%) and Y2 (75%) is

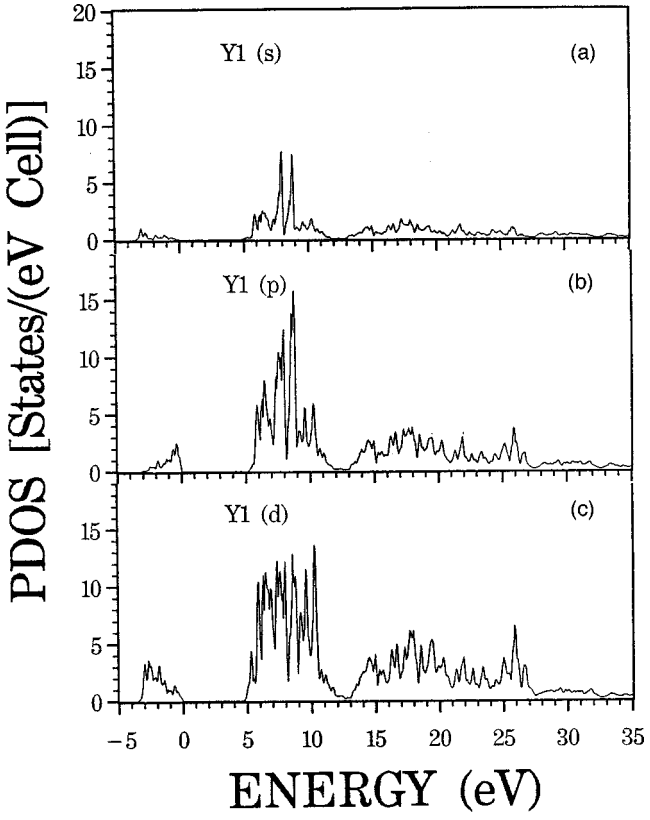

FIG. 5. Orbital-resolved PDOS of Y1. (a) s type. (b) p type. (c) d type.

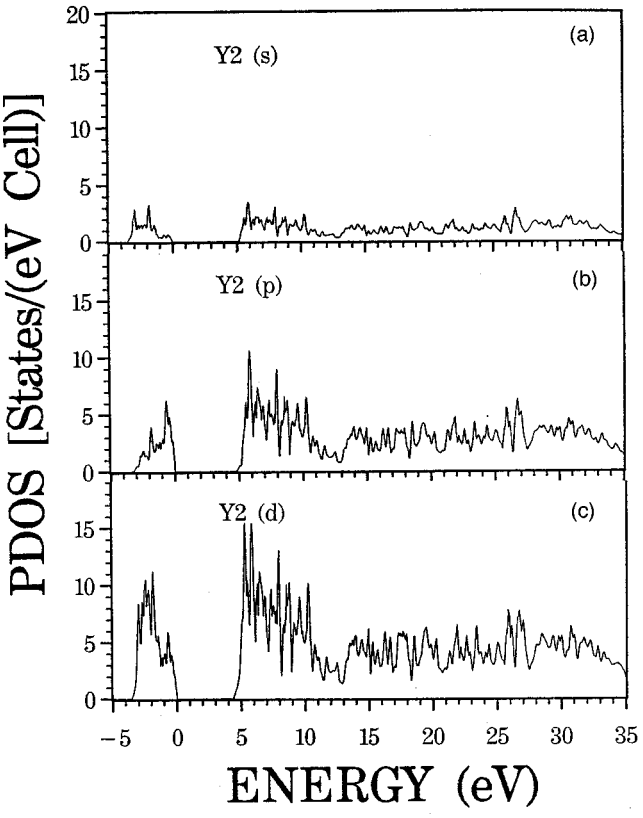

FIG. 6. Orbital-resolved PDOS of Y2. (a) s type. (b) p type. (c) d type.

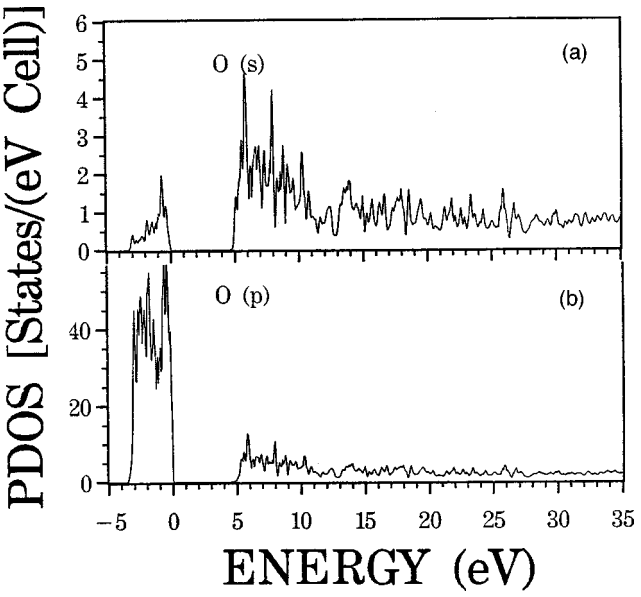

FIG. 7. Orbital-resolved PDOS of O. (a) *s* type. (b) *p* type.

rather small. However, it can still be observed that the spectral weight of Y2 $4d$ is shifted to the lower-energy side of the CB than the Y1 $4d$, and the Y2 has more states distributed above 27 eV. (4) The lower CB's up to 11 eV are predominately from Y $4d$ and Y $5p$. This part of the CB DOS is somewhat different from the previous minimal basis calculation.[11] The CB in the latter was dominated by Y $4d$ orbitals, separated into two parts by a gap. The lower part has contributions mainly from states of Γ_{12} symmetry. In the present calculation, the division of Y $4d$ CB into two parts is less clear because of the p-d mixing, although a clear dip in the PDOS at 8.2 eV is still present. This difference is of course due to the more extensive basis used in the present calculation, and the fact that Y1 and Y2 have slightly different PDOS's. We believe the present calculation of the total DOS is more accurate. However, its decomposition into partial components, which is based on the Mulliken scheme, is only approximate. This is especially true for the CB because of the extended nature of the basis function.

The above results are in general good agreement with XES, x-ray photoemission spectroscopy (XPS) and extended x-ray-absorption fine-structure (EXAFS) measurements on Y_2O_3.[12–14] Soft-x-ray emission spectroscopy provides information on the occupied VB DOS. The calculated Y $5p$ and O $2p$ PDOS's in the VB region are in close agreement with the Y M_v and O K emission spectra of Ref. 12. It is also in good agreement with the XPS data of Ref. 13, but the energy resolution in that work is rather low. Also, our calculated PDOS agrees quite well with the PDOS from the LMTO calculation.[12] The XAS edges of the Y K and Y $L_{\rm II}$ from the EXAFS measurements probe the unoccupied Y p and Y d PDOS in the CB region. The main features in the experimental data are the two peak structures separated by roughly 7 and 2.15 eV, respectively for the K and $L_{\rm II}$ edges.[13,14] These are in reasonable agreement with our calculations as shown in Figs. 5 and 6. If we further smooth the PDOS curves and take the center of gravity of the structure as the peak positions, we can roughly estimate the separation of the two parts in the Y $4d$ PDOS to be 2.3 eV. For the Y p PDOS in the CB, Y1 and Y2 show some differences. Still, the center of gravity of the lower group is around 6.5–8.5 eV, and the first recognizable structure at a higher energy is at 14.5 eV. The difference is about 7 ± 1.0 eV. The data for the O K edge from Ref. 13 show complex structures near the edge for both stoichiometric and reduced samples. The measurement on the stoichiometric sample was hampered by the charging effect, and the reduced sample contains as much as 10% of O vacancies. It is therefore difficult to compare with the results from the perfect crystal calculation. Our calculated O $2p$ PDOS's in the CB region show no major structures above 11 eV, which seems to be consistent with the data of Ref. 13.

TABLE I. Calculated Mulliken effective charges q^* in Y_2O_3 and α-Al_2O_3.

	Y_2O_3	α-Al_2O_3
Cation	+2.08 (Y1)	+1.89
	+2.10 (Y2)	
O	−1.39	−1.26

The calculated Mulliken effective charges and bond orders for Y_2O_3, according to Eqs. (1) and (2), are listed in Tables I and II, respectively. A minimal basis was used in this calculation. For comparison, similar values for α-Al_2O_3 are also listed. From the calculated effective charges, it can be seen that Y_2O_3 is far from being fully ionic, and that bonding between Y and O has a substantial covalent component. Only about one electron per Y atom is transferred to O. The effective charges on Y1 and Y2 are very similar, with Y1 smaller than Y2 by only 0.02 electron. These values are quite close to the ones based on a more elaborate real-space integration scheme,[11] in which an ionic formula of $Y_2{}^{+2.16}O_3{}^{-1.44}$ was suggested. The calculated bond order for Y_2O_3 and α-Al_2O_3 are listed in Table II. The bond order is a quantitative measure of the strength of the bond. We see that the bond orders for Y-O in Y_2O_3 and Al-O in α-Al_2O_3 are comparable, even though the Y-O bond lengths are longer than the Al-O bond length by more than 20%.

Figure 8 displays the calculated valence charge-density distributions in three crystallographic planes. The first is a (001) plane containing the O ions. The empty sites are the ''missing'' O of the minicubes discussed in Sec. II. There are considerable interactions between the O ions. The second plane is also a (001) plane, but contains Y1 and Y2 atoms. The slight difference between Y1 and Y2 is demonstrated here by noting the different bonding pattern with O planes-

TABLE II. Calculated bond order and bond distance d between pairs of atoms in perfect crystals of Y_2O_3 and α-Al_2O_3.

Y_2O_3		α-Al_2O_3	
d (Å)	$\rho_{i,j}$	d (Å)	$\rho_{i,j}$
2.261 (Y1)	0.098	1.857	0.105
2.249 (Y2)	0.104	1.969	0.083
2.278 (Y2)	0.092		
2.336 (Y2)	0.087		

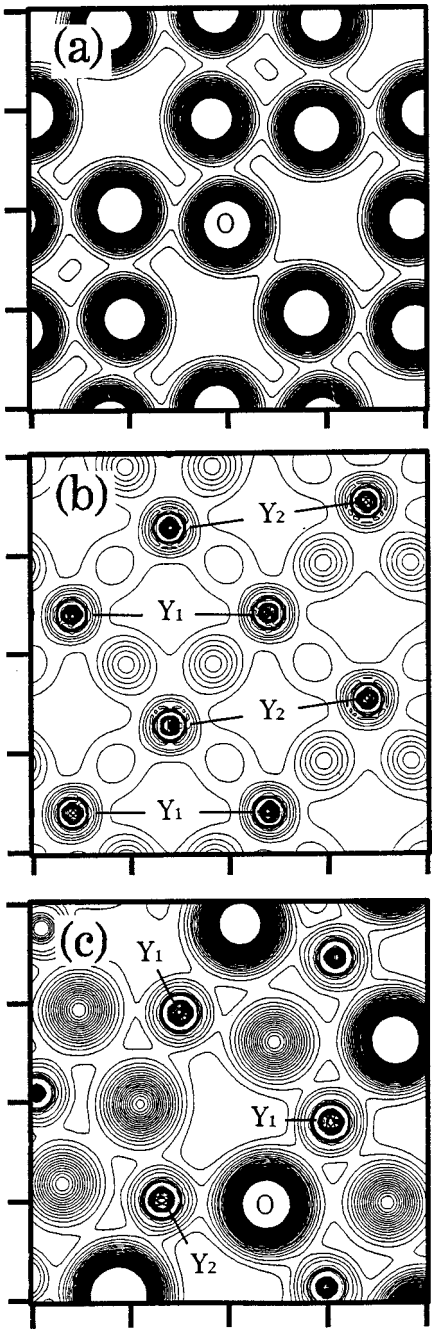

FIG. 8. Valence charge density contours in the (a) O plane and (b) Y plane, and (c) in a plane containing a Y1-O-Y2 bonding. The contour lines range from 0.01 to 0.25 electrons/(a.u.)^3 in intervals of 0.005.

above and below it. The third plane is a vertical one containing the Y1-O-Y2 bonding segment. The covalent character of the bonding is quite evident. The rather unique type of Y-O bonding in Y_2O_3 was discussed in Ref. 11.

B. Ground-state lattice properties

Figure 9 shows the calculated total energy as a function of crystal volume. Also shown is the volume dependence of the band gap E_g. Our calculation shows that the predicted equilibrium lattice constant underestimates the measured one by about 2.0%. Such a discrepancy is not unusual for LDA calculations. The energy vs V data were fitted to three different EOS's for the bulk modulus B and pressure coefficient B'. The results are summarized in Table III. The three EOS's gave close values for B. We believe the result based on the Burch-Murnagan EOS is more accurate, especially for B'. The calculated values compare favorably with the values of elastic modulus deduced from compressive measurements on densified polycrystalline samples of Y_2O_3.[15,30,31] It is noted that the experimental values are rather scattered. In the case of Y_2O_3, we tend to believe the calculated values for B and B' may be more reliable. In a similar calculation for α-Al_2O_3,[22] the calculated bulk modulus of 242 Gpa is in very close agreement with the measured data. Our calculation also indicates that Y_2O_3 is considerably softer than α-Al_2O_3. This may be related to the fact that the cubic structure of Y_2O_3 is less closely packed. Figure 8 shows large void spaces in both the O and Y sublattices.

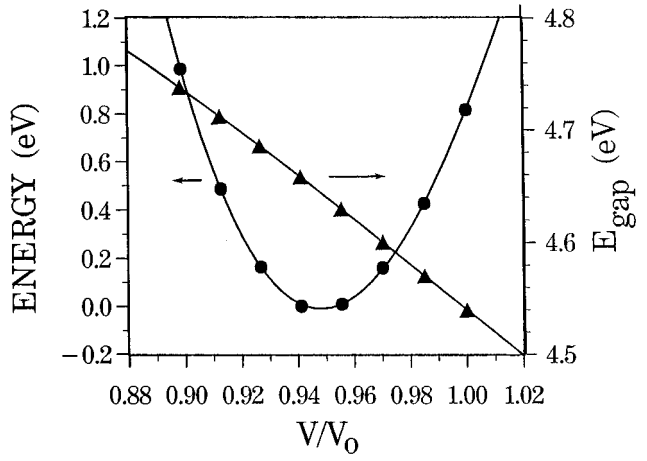

FIG. 9. Calculated total energy (left scale) and band gap E_g (right scale) vs V/V_0 in Y_2O_3. V_0 is the measured equilibrium volume taken to be 1192.36 Å^3 here.

Figure 9 also shows the band gap of Y_2O_3 increases with pressure. The increase is not strictly linear. It is estimated that near the calculated equilibrium volume, the rate of change in the gap, dE/dP is about 0.012 eV/Gpa. This rate of change is about a factor 5 smaller than found in the very hard materials such as β-C_3N_4 (Ref. 32) or diamond.[33]

C. Optical properties

The calculated optical properties of Y_2O_3 are presented in Fig. 10 in the form of (1) interband optical conductivity

TABLE III. Calculated bulk modulus and pressure coefficient of Y_2O_3 using different EOS's.

	B (Gpa)	B'
Fourth-order polynomial	180	6.92
Murnagan	182	7.65
Birch-Murnaghan	183	4.01
Expt.	150,[a] 170,[b] 57–177[c]	

[a]Reference 15.
[b]Reference 30.
[c]Reference 31.

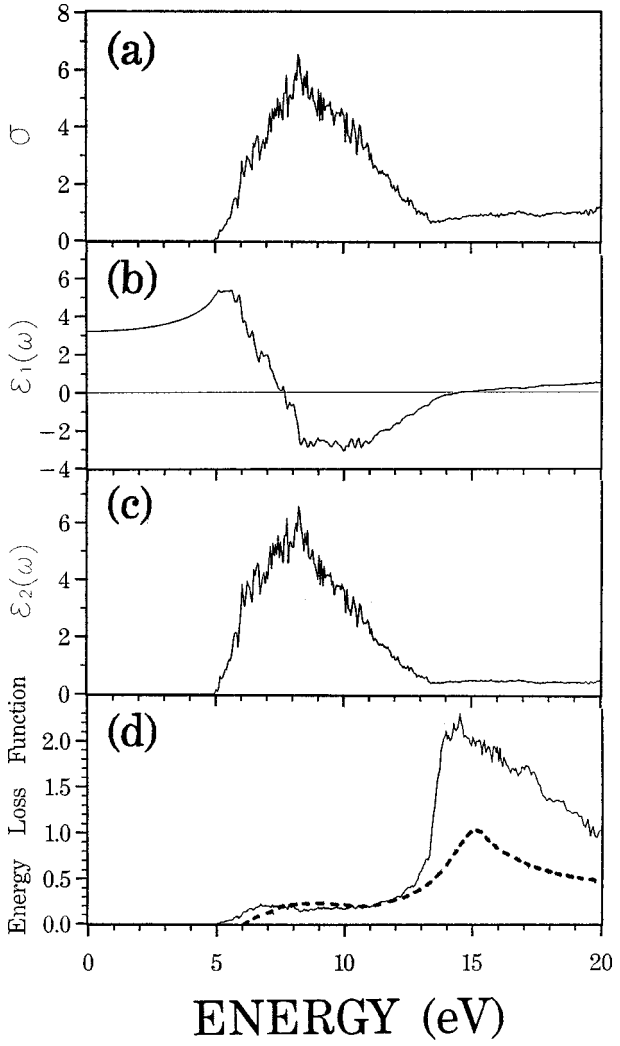

FIG. 10. Calculated optical properties of Y_2O_3: (a) $\sigma(\omega)$. (b) $\varepsilon_1(\omega)$. (c) $\varepsilon_2(\omega)$. (d) Energy-loss function. The dashed line in (d) is the experimental data of Ref. 9.

$\sigma(\omega)$, (2) real and imaginary parts of the dielectric function, and (3) the electron-energy-loss function. The calculations are limited to photon energy of 20 eV and less. Above 20 eV, transitions from the semicore Y $4p$ levels may become important. The calculated dielectric functions are in good agreement with the vacuum ultraviolet measurement of Tomiki *et al.*[10] on Y_2O_3 crystal more than 20 years ago. The experimental absorption threshold is at 5.5 eV compared to the calculated absorption edge at 5.0 eV, which is quite sharp, and the intrinsic band gap of 4.5 eV. This may indicate that the direct interband transition between the top of the VB and the single CB at Γ is symmetry forbidden. Our calculation seems to support the interpretation that the sharp peak observed experimentally near the absorption edge may be an excitonic peak. The presence of an excitonic peak generally sharpens the absorption edge. The major peak in the calculated optical spectrum for Y_2O_3 is at 8.0 eV, while the data of Tomiki *et al.*[10] show the major peak to be at 7.2 eV. Tomiki *et al.* also identified eight absorption structures in the 5–13-eV region. Although, there are also many smaller structures in the calculated $\varepsilon_2(\omega)$ curve in the same region, a one-to-one correspondence with the experimental structures appears to be difficult. Figure 10(d) also shows the experimental electron-energy-loss (EEL) spectrum of Ref. 9. The agreement with the calculated one below 13 eV is very good. Above 13 eV, the theoretical EEL spectrum has a much higher amplitude, although the shape of the curve is quite well reproduced. Since both $\varepsilon_1(\omega)$ and $\varepsilon_2(\omega)$ are fairly small above 13.0 eV, the uncertainty in the calculated EEL spectrum can be magnified. The main peak in the EEL spectrum is interpreted as the bulk-plasmon frequency ω_p. The calculated ω_p is 14.5 eV, while the experimental ω_p is 15 eV.

From the $\varepsilon_1(\omega)$ curve of Fig. 10(b), it can be seen that the electronic part of the static dielectric constant in the zero-frequency limit is about 3.20. This value is in fairly good agreement with the refractive index measurement. Nigara[7] measured the refractive index of Y_2O_3 within the $1000-5000\text{-cm}^{-1}$ region. In the gap region, Fig. 7 of Ref. 7 shows the refractive index to be about 1.9, which suggests an $\varepsilon_1(\omega)$ value at this range of frequency to be about 3.6, in quite good agreement with the theoretical value of $\varepsilon_1(\omega) = 3.50$ at $h\omega = 2.0$ eV.

V. CONCLUSIONS

In this paper, we presented detailed results of the electronic structure and optical properties of the Y_2O_3 crystal. Also calculated are the ground-state structural properties. The calculated results are in general agreement with a variety of experimental data including XES and EXAFS for the orbital-projected PDOS. In some cases, we believe the calculated results to be more reliable then the measured ones, considering the difficulty in obtaining pure, simple crystalline samples for Y_2O_3. It is also shown that Y_2O_3 can not be considered as a highly ionic crystal. It is softer, and has a smaller band gap than α-Al_2O_3. The CB is dominated by the Y $4d$ states, and the CB edge consists of a single band. The direct optical transition at Γ may be symmetry forbidden. Hence the optical-absorption edge is larger then the intrinsic band gap by about 0.5 eV. A static dielectric constant of 3.20, and a plasmon frequency at 14.5 eV, are obtained.

With the electronic structure and bonding in Y_2O_3 and α-Al_2O_3 reasonably well understood, it is now feasible to carry out first-principles studies on the defect structures in Y_2O_3, or with Y as an impurity in other ceramic oxides. The OLCAO method used in the present study is quite well suited to such studies.[25,26] It is also fruitful to study the intermediate phases of YAP, YAG, and YAM formed between Y_2O_3 and Al_2O_3. For example, in the garnet structure, the cations occupy fourfold-, sixfold-, and eightfold-coordination positions of various bond lengths. Such studies are currently being carried out;[34] and will further our understanding of the electronic structure and properties of this important class of refractory and optical materials.

ACKNOWLEDGMENT

This work was supported by the U.S. Department of Energy under Grant No. DE-FGO2-84DR45170, and by UMRB and UMKC EPIP Grants.

*Author to whom correspondence should be addressed.

[1] M. K. Loudjani, A. M. Huntz, and R. Cortés, J. Mater. Sci. **28**, 6466 (1993).
[2] A. M. Thompson, K. K. Soni, H. M. Chan, M. P. Harmer, D. B. Williams, J. M. Chabala, and R. Levi-Srtti, J. Am. Ceram. Soc. **80**, 373 (1997).
[3] F. A. Golightly, F. H. Scott, and G. C. Wood, J. Oxid. Mater. **10**, 163 (1976).
[4] E. Schumann, J. C. Yang, M. J. Graham, and M. Rühle, Mater. Corrosion **46**, 218 (1995).
[5] C. Brecher, G. C. Wei, and W. H. Rhodes, J. Am. Ceram. Soc. **73**, 1473 (1990).
[6] T.-I. Mah, K. A. Keller, S. Sambasivan, and R. J. Keraus, J. Am. Ceram. Soc. **80**, 874 (1997).
[7] Y. Nigara, J. Appl. Phys. **7**, 404 (1968).
[8] V. N. Abramov and A. I. Kunznetsov, Fiz. Tverd. Tela (Leningrad), **20**, 689 (1978) [Sov. Phys. Solid State **20**, 399 (1978)].
[9] J. Frandon, B. Brousseau, and F. Pradal, Phys. Status Solidi B **98**, 379 (1980).
[10] T. Tomiki, J. Tamashiro, Y. Tanahara, A. Yamada, H. Fukutani, T. Miyahara, H. Kato, S. Shin, and M. Ishigame, J. Vac. Sci. Technol. B **55**, 4543 (1986).
[11] W. Y. Ching and Y.-N. Xu, Phys. Rev. Lett. **65**, 895 (1990).
[12] D. R. Mueller, D. L. Ederer, J. van Ek, W. L. O'Brien, Q. Y. Dong, J. Jia, and T. A. Callcott, Phys. Rev. B **54**, 15 034 (1996).
[13] F. Jollet, C. Noguera, N. Thromat, M. Gautier, and J. P. Duraud, Phys. Rev. B **42**, 7587 (1990).
[14] N. Thromat, C. Noguera, M. Gautier, F. Jollet, and J. P. Duraud, Phys. Rev. B **44**, 7904 (1991).
[15] Ö. Ünal and M. Akinc, J. Am. Ceram. Soc. **79**, 805 (1996).
[16] H. Ishibash, K. Shimomoto, and K. Nakahigashi, J. Phys. Chem. Solids **55**, 809 (1994).
[17] H. O'Conner and T. M. Valentine, Acta Crystallogr., Sect. B: Struct. Crystallogr. Cryst. Chem. **24**, 1968 (1969).
[18] L. Smrcok,Crystal Res. Technol. **24**, 607 (1989).
[19] R. W. G. Wyckoff, in *Crystal Structure* (Interscience, New York, 1966), Chap. 5, p. 5.
[20] W. Y. Ching, J. Am. Ceram. Soc. **73**, 3135 (1990).
[21] Y.-N. Xu and W. Y. Ching, Phys. Rev. B **43**, 4461 (1991).
[22] W. Y. Ching and Y.-N. Xu, J. Am. Ceram. Soc. **77**, 404 (1994).
[23] S. Loughin, R. H. French, W. Y. Ching, Y.-N. Xu, and G. A. Slack, Appl. Phys. Lett. **63**, 1182 (1993).
[24] Y.-N. Xu and W. Y. Ching, Phys. Rev. B **51**, 17379 (1995).
[25] Y.-N. Xu, Z.-Q. Gu, X.-F. Zhong, and W. Y. Ching, Phys. Rev. B **56**, 7277 (1997).
[26] W. Y. Ching, Y.-N. Xu, and M. Rühle, J. Am. Ceram. Soc. (to be published).
[27] R. S. Mulliken, J. Am. Chem. Soc. **77**, 887 (1954); **23**, 1833 (1955); **23**, 1841 (1955).
[28] F. D. Murnagan, Proc. Natl. Acad. Sci. USA **30**, 244 (1944).
[29] F. Birch, J. Geophys. Res. **83**, 1257 (1957).
[30] W. R. Manning, O. Hunter, and B. R. Powell, J. Am. Ceram. Soc. **52**, 436 (1969).
[31] G. A. Gogotsi, Ceramurgia. Int. **6**, 31 (1980).
[32] H. Yao and W. Y. Ching, Phys. Rev. B **50**, 11 231 (1994).
[33] S. Fahy, K. J. Chang, S. G. Louie, and M. L. Cohen, Phys. Rev. B **35**, 5856 (1987).
[34] W. Y. Ching and Y.-N. Xu (unpublished).